

# Temperature-dependent barrier height inhomogeneities in PTB7:PC<sub>71</sub>BM-based organic solar cells

Brahim Ait Ali<sup>1,2</sup>, Reda Moubah<sup>2,†</sup>, Abdelkader Boulezhar<sup>1</sup>, and Hassan Lassri<sup>2</sup>

<sup>1</sup>LERDyS, Faculty of Science Ain Chock, Hassan II University of Casablanca, Morocco

<sup>2</sup>LPMMAT, Faculty of Science Ain Chock, Hassan II University of Casablanca, Morocco

(Received 16 December 2019; revised manuscript received 16 June 2020; accepted manuscript online 15 July 2020)

We report on the temperature-dependent Schottky barrier in organic solar cells based on PTB7:PC<sub>71</sub>BM. The ideality factor is found to increase with temperature decreasing, which is explained by a model in which the solar cell is taken as Schottky barrier diode. Accordingly, the dark current in the device originates from the thermally emitted electrons across the Schottky barrier. The fittings obtained with the thermal emission theory are systematically studied at different temperatures. It is concluded that the blend/Ca/Al interface presents great inhomogeneity, which can be described by 2 sets of Gaussian distributions with large zero bias standard deviations. With the decrease of temperature, electrons favor going across the Schottky barrier patches with lower barrier height and as a consequence the ideality factor significantly increases at low temperature.

**Keywords:** organic materials, photovoltaics, Schottky barrier, barrier height

**PACS:** 88.40.jr, 78.55.Kz, 73.30.+y, 33.15.Hp

**DOI:** 10.1088/1674-1056/aba5fc

## 1. Introduction

Silicon is broadly utilized in the manufacture of electronic devices. Nevertheless, the market needs devices with a low industrial price and permitting the design of devices on big areas and bendable supports.<sup>[1]</sup> Solar cells based on organic semiconductors validate these requirements.<sup>[2,3]</sup> However, intense researches are still performed to investigate the practicability of putting it on the market in terms of yield and reliability. Besides the attraction due to cheap cost,<sup>[4]</sup> easy to handle and degradability, organic semiconductors guarantee clean technology.<sup>[5]</sup> These interesting properties have made organic semiconductors very promising materials for research laboratories and manufacturers around the world,<sup>[6,7]</sup> provoking quick growth in the field of organic electronics.<sup>[8]</sup> For photovoltaic applications and for organic semiconductors, the charge transport mechanisms are controlled by bulk process, and the semiconductor/electrode interface can affect the charge transport. Thermoelectronic emission, Schottky effect and effect emission tunnel can be used to describe the mechanisms which are governed by the interface.<sup>[9]</sup> By applying an electric field, the charges can be injected into the conduction band beyond potential barrier, where the current density obeys the Richardson-Schottky law.<sup>[9]</sup> One can notice that in the conventional bulk-heterojunction architecture, it was recently shown that the blend/cathode Schottky junction serves as the essential diode for the photovoltaic function.<sup>[10]</sup> However, up to now few researches have focused on such junctions, and their physical properties are not well-understood.<sup>[10]</sup> In this work, the electrical charge transport in

the dark and under the illumination conditions are studied in the blend of poly[[4,8-bis[(2-ethylhexyl)oxy]benzo[1,2-b:4,5-b']dithiophene-2,6-diyl][3-fluoro-2-[(2-ethylhexyl)carbonyl]thieno[3,4-b]thiophenediyl]] (PTB7) and [6,6]-Phenyl-C<sub>71</sub>-butyric acid methyl ester (PC<sub>71</sub>BM)-based device (as shown in Fig. 1(a)),<sup>[2,11,12]</sup> with the temperature dependence of  $J$ - $V$  features. The temperature dependence of the junction diode is studied as well.

## 2. Experimental details

PTB7 was purchased from 1-material and PC<sub>71</sub>BM from solenne. We have used glass substrates with a 4-mm stripe of ITO which were cleaned with acetone, propane-2-ol and plasma ashing. PTB7:PC<sub>71</sub>BM-based solar cells were fabricated using the blend of PTB7:PC<sub>71</sub>BM dissolved in a solution of 25 mg/ml in 1,2-dichlorobenzene, in which we have added 3-vol% diiodooctane to the solution. Spin coating was utilized to deposit a layer of the poly(3,4-ethylene dioxythiophene) (PEDOT) and poly(4-styrenesulfonic acid) (PSS) which forms the PEDOT:PSS,<sup>[13]</sup> which was dried at 120 °C for 10 min. The rotation speed was 1000 rpm which gives rise a film thickness of 80 nm. Then, the active layer was solution cast and put in a nitrogen glove box for drying the whole night. A semi-transparent top contact comprised of 15nm-thick Ca film and 15nm-thick Al film was deposited using thermal evaporation (as shown in Fig. 1(b)). Three pixels with an area of 8 mm<sup>2</sup> were determined by the overlap of the anode and cathode. More details about the preparation techniques can be found in Refs. [14,15].

<sup>†</sup>Corresponding author. E-mail: [reda.moubah@hotmail.fr](mailto:reda.moubah@hotmail.fr)

A class A, sciencetech solar simulator was used for solar cells measurements. The intensity was calibrated using an ORIEL reference cell using KG5 filter. The spectral mismatch factor was around 0.995 for PTB7:PC<sub>71</sub>BM and not corrected. An aperture of similar dimension as the pixel was utilized to remove contribution from stray light outside the device.

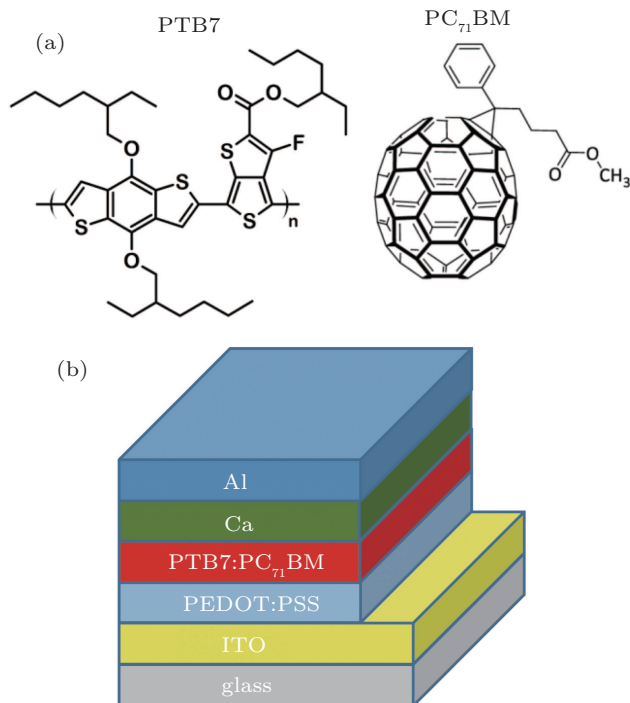


**Fig. 1.** (a) Chemical structures of components in active layer and (b) device structure.

### 3. Results and discussion

#### 3.1. Current–voltage characteristics as a function of temperature

The  $J$ – $V$  curve exhibits the features of PTB7:PC<sub>71</sub>BM-based solar cells.<sup>[16,17]</sup> The dark and light  $J$ – $V$  curves recorded at various temperatures are displayed in Fig 2. It is found that the density of current in light is greater than that in the dark, which is related to the increase of the excitons created by light.

To extract the reverse dark saturation current density ( $J_s$ ) and the ideality factor  $n$ , we fit the  $J$ – $V$  data (Fig. 2(a)) using the following equation:<sup>[18]</sup>

$$J = \frac{R_{sh}}{R_s + R_{sh}} \left\{ J_s \left[ \exp \left( \frac{e(V - JR_s)}{nkT} \right) - 1 \right] \right\}, \quad (1)$$

where  $R_{sh}$  and  $R_s$  are the shunt and series resistance of the device, respectively,  $k$  is the Boltzmann constant and equal to  $1.38 \times 10^{-23}$  J/K or  $8.61 \times 10^{-5}$  eV/K,  $e$  is the elementary charge, and  $n$  is the ideality factor of the device and it was extracted from the slope of  $\log(J)$ – $V$  plot in the dark (where  $V > 3kT/e$ ) at different temperatures. At low positive voltages, the shunt resistance controls the  $J$ – $V$  characteristics while at the intermediate voltages, the series resistance

does not affect the  $J$ – $V$  dependence and the  $J$ – $V$  characteristics show a diode behavior.<sup>[10–12]</sup> We fit the  $J$ – $V$  data recorded in the dark at the low and intermediate applied voltages. In this case, the ideality factor  $n$  can be obtained from the slope of the linear region of  $\log(J)$ – $V$  curve, and can be written as  $n = (e/kT) [dV/d \log(J)]$ .<sup>[21]</sup> It is found that  $n$  significantly increases with temperature decreasing (see Fig. 3). The magnitude of  $n$  is much larger than 2. One possible process contributing to large ideality factor is high level injection in resistive material. An alternative explanation for the large ideality factor is multi-level recombination process where high defect density plays a critical role in providing the coupled recombination paths within defect states. As a result, coupled defect centers will increase recombination rate in the material, thereby increasing ideality factor to  $n > 2$ .<sup>[2,13]</sup> We note that  $J_s$  shows an interesting tendency with the increase of temperature: first it slightly decreases and then sharply increases. Usually for an ideal Schottky junction, both the Schottky barrier height and the built-in voltage on the semiconductor side should increase with temperature decreasing.<sup>[23]</sup> At low temperature, high-energy carriers that can overcome the Schottky barrier height become less and less, which should reduce  $J_s$  with the decrease of temperature, the large  $n$  values and the abnormal  $J_s$  behavior with the decrease of temperature indicate that the Schottky junction is not ideal.

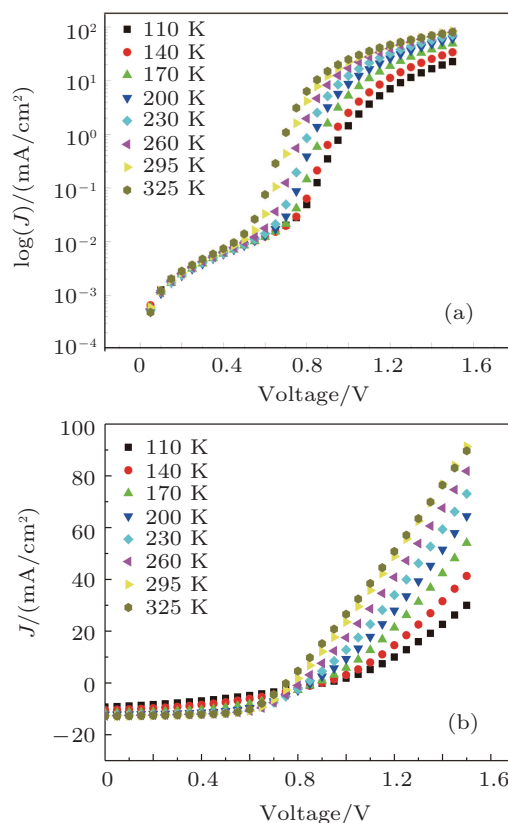


**Fig. 2.** (a)  $\log(J)$ – $V$  (voltage) of PTB7:PC<sub>71</sub>BM-based device in the dark, and (b) the  $J$ – $V$  characteristics under illumination in temperature range of 110 K–325 K.

We introduce a Schottky barrier (SB) diode model. Ac-

tually this model has also been used in OSCs by other groups and has been proven to fit well with the experimental results. In this model, the blend of donor and acceptor is considered as a p-type semiconductor (in the case of a conjugated polymer, it is usually p-doped when exposed to air or moisture).<sup>[9]</sup>

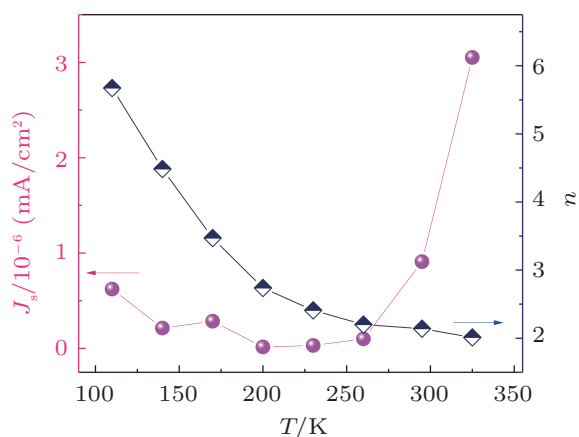


Fig. 3. Plot of  $n$  and  $J_s$  versus temperature (extracted from  $J$ - $V$  curves in the dark) of the investigated device at various temperatures.

The parameters  $V_{OC}$ ,  $J_{SC}$ , and FF (extracted under illumination) are plotted in Fig. 4. As shown in Fig. 4(a),  $V_{OC}$  displays a linear increase with temperature decreasing at a slope of  $-0.715$  mV/K under 1 sun of intensity. It is accepted that  $V_{OC}$  of organic material-based solar cells depend on the difference between the highest occupied molecular orbital (HOMO) of the donor and the lowest unoccupied molecular orbital (LUMO) of the acceptor.<sup>[15,16]</sup> Scharber *et al.*<sup>[26]</sup> have investigated the correlation between the energy levels of the donor-acceptor blend and the  $V_{OC}$  of BHJ cells based on 26 different BHJ systems. Accordingly, it can be deduced that the  $V_{OC}$  of BHJ cell can be expressed as

$$V_{OC} = \frac{1}{e} (|E_{HOMO,D}| - |E_{LUMO,A}| - 0.3eV), \quad (2)$$

where  $E_{HOMO,D}$  is the HOMO level of the donor and  $E_{LUMO,A}$  is the LUMO level of the acceptor. It should be noted that

the  $V_{OC}$  loss (0.3 V) is empirical. In our device, the HOMO level and LUMO level of PTB7 donor and PC<sub>71</sub>BM acceptor are  $-5.15$  eV and  $-3.9$  eV, respectively.<sup>[27]</sup> Substitution of these values into Eq. (2) can calculate  $V_{OC}$  at room temperature which is found to be 0.95 eV, it is slightly different from the experimental value ( $V_{OC} \approx 0.78$  eV at 295 K). Shockley and Queisser<sup>[28]</sup> suggested that unavoidable radiative recombination fixed an upper limit to  $V_{OC}$ . Recombination independent of its kind annihilates the carriers which induces energy loss, and thus  $V_{OC}$  decreases. Previous investigation has reported that the recombination mechanism can vary from monomolecular state at short circuit to bimolecular state at open circuit<sup>[15,20]</sup> in which  $V_{OC}$  can be given by

$$e \cdot V_{OC} = E_g - \frac{\sigma^2}{kT} - kT \left( \frac{N_n N_p}{n \cdot p} \right), \quad (3)$$

where  $\sigma$  characterizes the width of the Gaussian density of states (DOS),  $N_n$  ( $N_p$ ) is the effective conduction band (valence band) DOS,  $n$  and  $p$  are the electron and hole concentration, respectively, and  $kT$  is the thermal energy. There are 3 terms on the right-hand side of Eq. (3): the 1st term is associated with the effective bandgap  $E_g = |E_{HOMO,D}| - |E_{LUMO,A}|$ ; the 2nd term shows the disorder-induced  $V_{OC}$  loss, and the 3rd term is the carrier recombination-induced  $V_{OC}$  loss. If  $T$  is higher than 110 K, the 3rd term becomes dominant in Eq. (3) (Fig. 4(a)), since  $V_{OC}$  does change almost linearly with temperature. In the PTB7:PC<sub>71</sub>BM BHJ cells, we can regard the 2nd term as zero, thus the  $V_{OC}$  is fitted by using a classical linear equation and finally, it can be written as  $V_{OC} = -7.15 \times 10^{-4}T + 0.98$ , which is an expression of a fit straight. The diminution of  $V_{OC}$  with temperature increasing can be understood by considering the carrier recombination in the PTB7:PC<sub>71</sub>BM BHJ cells which becomes more important with the temperature rising.

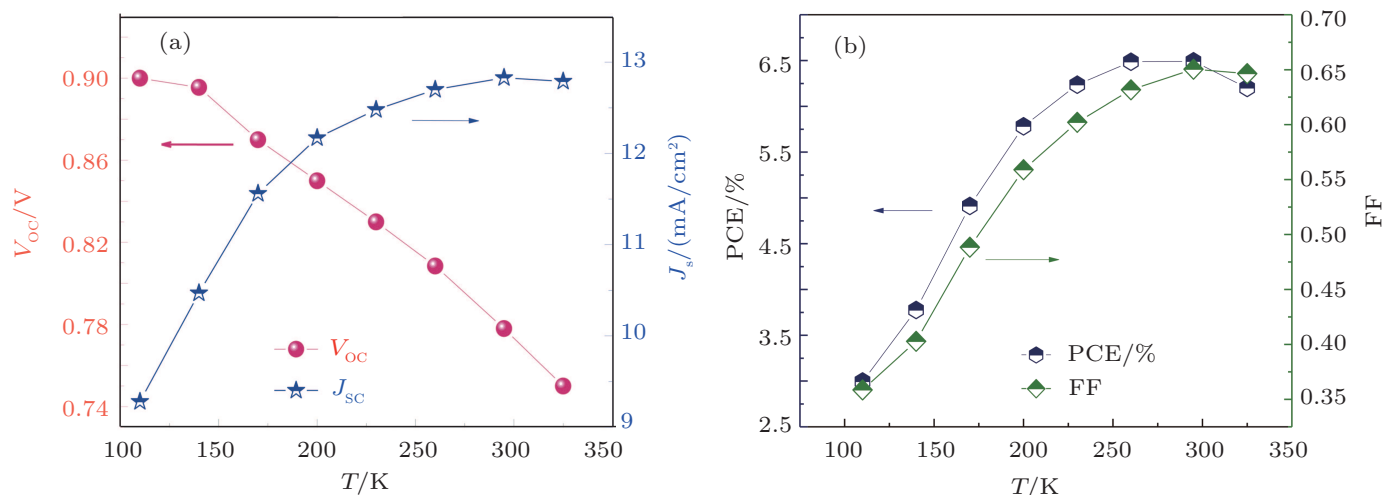


Fig. 4. Variations of (a)  $V_{OC}$  and  $J_{SC}$ , (b) PCE (%) and fill factor (FF) with temperature of the investigated device.

In addition,  $J_{SC}$  linearly increases with operating temperature increasing. The enhancement of  $J_{SC}$  should be ascribed to the improvement of the carrier (hole and electron) mobility and thus improving the photocurrent extraction at elevated temperature. The fill factor (FF) of the PTB7:PC<sub>71</sub>BM cell shows a linear increase with operating temperature increasing. The improvement of FF can be explained by the enhanced charge extraction due to the increased carrier mobility and improved active layer/cathode contact at elevated temperature leading the series resistance to decrease significantly, which affects the fill factor.

Figure 4(b) shows the temperature behavior of the power conversion efficiency (PCE). Analysis of the temperature dependence of photovoltaic reveals that the value of the power conversion efficiency (PCE) increases with temperature increasing and it stabilizes at high temperature. This behavior can be attributed to the increase in  $J_{SC}$  which can be more than the offset corresponding decrease in  $V_{OC}$ .<sup>[30,31]</sup>

### 3.2. Temperature-dependent Schottky barrier and Gaussian distribution

Figure 2(a) shows the characteristic curves of semi-logarithmic current density ( $\log J$ ) versus forward bias  $V$  measured in a temperature range of 110 K–325 K. The characteristic curves of a Schottky diode are given by Eq. (1) through using thermal emission (TE) theory, the dark saturation current density  $J_s$  can be written as follows:<sup>[23–25]</sup>

$$J_s = A^* T^2 \exp\left(-\frac{\Phi_{B0}}{kT}\right), \quad (4)$$

where  $A^*$  is the effective Richardson constant (assuming  $A^* = 120 \text{ A} \cdot \text{cm}^{-2} \cdot \text{K}^{-2}$ ) and  $\Phi_{B0}$  is the zero bias Schottky barrier height (SBH) (in unit eV). It can be re-expressed as the following expression

$$\ln\left(\frac{J_s}{T^2}\right) = \ln(A^*) - \frac{\Phi_{B0}}{kT}. \quad (5)$$

We extract the Schottky barrier height from the forward bias region. The temperature dependence of the barrier height determined from  $J$ – $V$  measurements is shown in Fig. 5.

It can be seen that the Schottky barrier height exhibits strong temperature dependence. The value of  $\Phi_{B0}$  increases from 0.33 eV to 1.01 eV as the temperature increases from 110 K to 325 K. we know that for an ideal Schottky junction, the barrier height usually should increase with temperature decreasing.<sup>[23,34]</sup> The anomalous behaviors of both the SBH and ideality factor are commonly observed in real Schottky contacts and can be related to the spatially inhomogeneous

Schottky barrier observed in real Schottky contacts and can be related to the spatially inhomogeneous Schottky barrier.<sup>[36]</sup> Using high resolution transmission electron microscope (HR-TEM), Janardhanam *et al.*,<sup>[37]</sup> have shown the presence of a non-uniform interfacial layer in the Se/Ge interface, which results from an interfacial reaction between Se and Ge occurring during Se deposition. Such a non-uniform interfacial layer is attributed to a combination of low and high barrier patches at the interface, responsible for spatially inhomogeneous Schottky barrier. Likewise, the presence of a non-uniform interfacial layer between active layer and electrode in this research might produce an inhomogeneous Schottky barrier due to the large surface roughness induced by the spin coating process. Since current transport at the metal–semiconductor interface is a temperature activated process, electrons at low temperatures can surmount the lower barriers and therefore, current transport will be dominated by current flowing through the patches of small regions with a lower SBH and a larger ideality factor.<sup>[25,26]</sup> By increasing temperature, more electrons have sufficient energy to surmount the higher Schottky barrier. As a result, the dominant barrier height will increase with temperature rising. The relatively large ideality factor is attributed to the presence of barrier height inhomogeneity at the interface, the presence of a thin interfacial native oxide layer and the formation of interfacial states.<sup>[25,26]</sup>

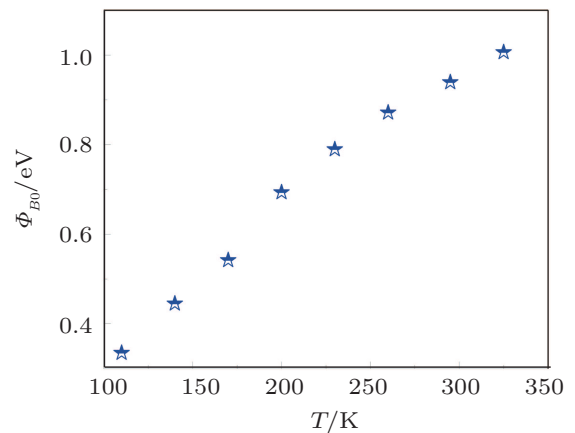
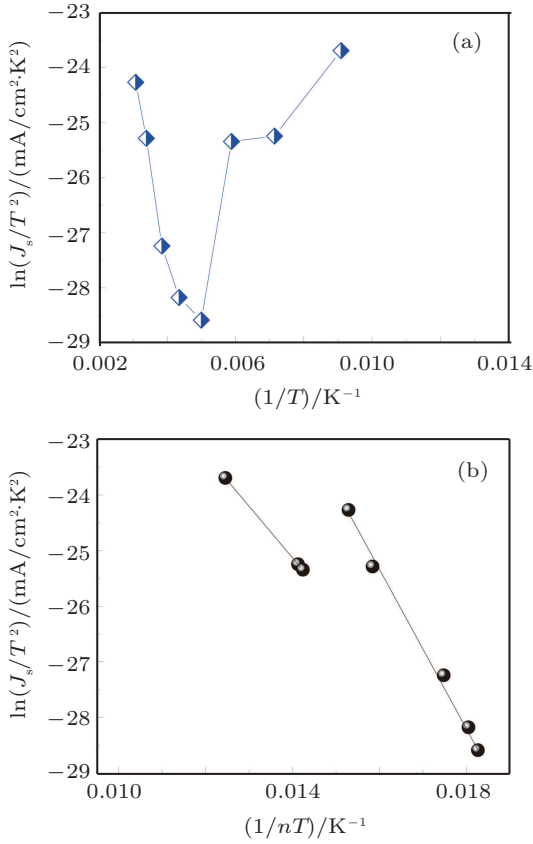


Fig. 5. Barrier height versus  $T$  of the investigated device.

Using the values of the saturation current density  $J_s$  at each temperature obtained from the dark current density–voltage ( $\ln J$ – $V$ ) data as shown in Fig. 2(a), the conventional Richardson plot of  $\ln(J_s/T^2)$  versus  $1/T$  is obtained in a temperature range of 110 K–325 K.

As can be observed in Fig. 6,  $\ln(J_s/T^2)$  does not change linearly with  $1/nT$  but not with  $1/T$ . This can be understood by considering the temperature-dependent barrier height and ideality factor due to the lateral inhomogeneity of the metal–semiconductor Schottky barrier heights.<sup>[27,28]</sup> One can notice

that the change of  $\ln(J_s/T^2)$  with  $1/nT$  presents 2 straight lines suggesting that two sets of Gaussian distributions of Schottky barrier higher in the contact area do exist.



**Fig. 6.** The plots of  $\ln(J_s/T^2)$  as a function of  $1/T$  [panel (a)] and  $1/nT$  [panel (b)].

Generally, the distribution of Schottky barrier energy levels can be depicted by the Gaussian distribution as follows:

$$P(\Phi_B) = \frac{1}{\sigma_0\sqrt{2\pi}} \exp\left[-\frac{(\Phi_B - \tilde{\Phi}_{B0})^2}{2\sigma_0^2}\right]. \quad (6)$$

The overall current density across the interface is calculated by integrating the current transporting through the Schottky barrier with different heights as follows:

$$J(V) = \int_{-\infty}^{\infty} J(\Phi_B, V) P(\Phi_B) d\Phi_B. \quad (7)$$

The barrier height with a Gaussian distribution can be expressed as<sup>[29,30]</sup>

$$\Phi_{B0} = \hat{\Phi}_{B0} - \frac{\sigma_s^2}{2kT}, \quad (8)$$

where  $\Phi_{B0}$  is the mean barrier height (in unit eV),  $\sigma_s$  (in unit eV) is the zero bias standard deviation of the Schottky barrier height distribution: the more inhomogeneous the barrier, the large the value of  $\sigma_s$  is. From Eq. (5),  $\hat{\Phi}_{B0}$  and  $\sigma_s$  can be obtained by fitting the  $\Phi_{B0}$  versus  $1/2kT$  curve (Fig. 7) with the intercept being  $\hat{\Phi}_{B0}$  and the slope being  $\sigma_s^2$ .

It is seen that the  $\Phi_{B0}$  versus  $1/2kT$  plot (Fig. 7) has two linear regions, which correspond to two Gaussian distributions of barrier heights at two different temperature ranges as described previously. The extracted  $\hat{\Phi}_{B0}$  and  $\sigma_s$  are found to be  $\hat{\Phi}_{B0} = 1.49$  eV and  $\sigma_s = 0.166$  eV in the high temperature range (200 K–325 K) and  $\hat{\Phi}_{B0} = 0.91$  eV and  $\sigma_s = 0.104$  eV in the low temperature range of 110 K–170 K. One can notice that the value of  $\sigma_s$  at high temperatures is larger than that at low temperatures, indicating the large interface inhomogeneity of the blend/Ca/Al contacts. At high temperatures, the cell presents much greater  $\hat{\Phi}_{B0}$  and  $\sigma_s$  than at low temperatures, which should originate from the enhanced thermal oscillation of the interface atoms and molecules.

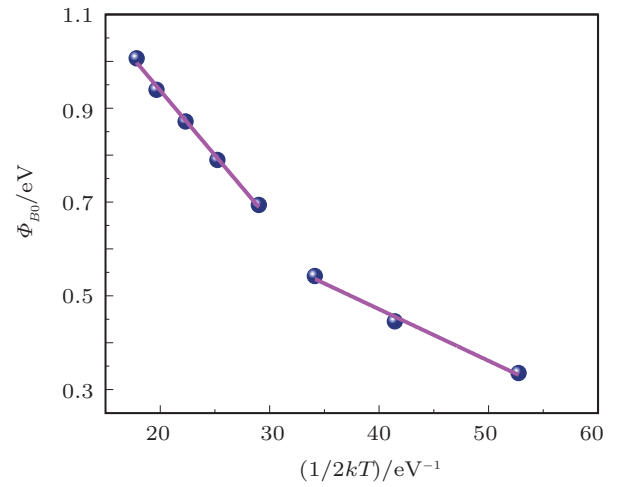


**Fig. 7.** Barrier height versus  $1/2kT$  of the investigated device.

Thus, we adopt the modified Richardson plot, taking into account the barrier inhomogeneity. The modified Richardson plot is given by

$$\ln\left(\frac{J_s}{T^2}\right) - \left(\frac{\sigma_s^2}{2k^2T^2}\right) = \ln(A^*) - \frac{\hat{\Phi}_{B0}}{kT}. \quad (9)$$

The  $\ln(J_s/T^2) - \sigma_s^2/(2k^2T^2)$  versus  $1/kT$  (Fig. 8) presents two linear variations with two slopes related to the zero-bias mean  $\hat{\Phi}_{B0}$  (Table 1):  $\hat{\Phi}_{B0} = 0.91$  eV (in the temperature window of 110 K–170 K) and  $\hat{\Phi}_{B0} = 1.49$  eV (from 200 K to 325 K). These obtained  $\hat{\Phi}_{B0}$  are very close to the ones determined from  $\Phi_{B0}$  versus  $1/2kT$  in Fig. 7 and the extracted  $A^*$  which is about  $120 \text{ A} \cdot \text{cm}^{-2} \cdot \text{K}^{-2}$  in line with that previously used (see Table 1).

**Table 1.** The  $\hat{\Phi}_{B0}$  (in unit eV) and  $A^*$  (in unit  $\text{A} \cdot \text{cm}^{-2} \cdot \text{K}^{-2}$ ) obtained from Eq. (9).

Cathode	Ca/Al	
Temperature range	$\hat{\Phi}_{B0}/\text{eV}$	$A^*/\text{A} \cdot \text{cm}^{-2} \cdot \text{K}^{-2}$
High (200 K–325 K)	1.49	135.64
Low (110 K–170 K)	0.91	169.01

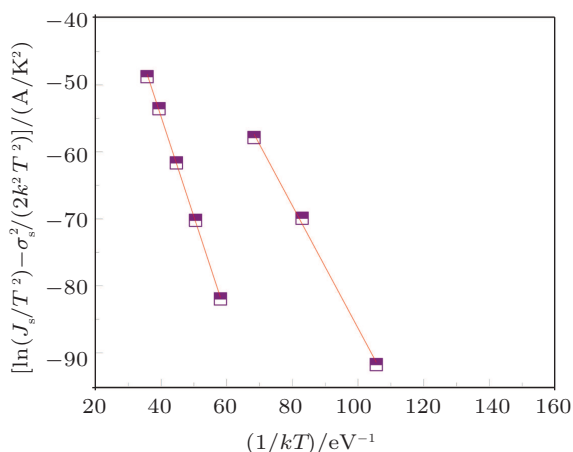


Fig. 8.  $\ln(J_s/T^2) - \sigma_s^2/(2k^2T^2)$  versus  $1/kT$  of the investigated device.

#### 4. Conclusions

In this work, we study the temperature-dependent Schottky barrier in organic solar cells based on PTB7:PC<sub>71</sub>BM. It is found that the ideality factor of the device obviously increases with temperature decreasing. In order to explain this phenomenon, a model is introduced in which the solar cell is taken as Schottky barrier diode. According to this model, the dark current in the device originates from the thermally emitted electrons across the Schottky barrier. By fitting with the TE theory the temperature dependence is systematically studied, demonstrating that the blend/Ca/Al Schottky barrier presents great inhomogeneity, which can be described by 2 sets of Gaussian distributions with large zero bias standard deviations. At low temperatures, electrons favor going across the Schottky barrier patches with lower barrier height, and as a result, the ideality factors shows a significant increase at low temperatures.

#### References

- [1] Zhang H, Zhang Q, Zhang Qi, Sun H, Hai G, Tong J, Xu H and Xia R 2019 *Chin. Phys. B* **28** 078108
- [2] Qi H X, Yu B H, Liu S, Zhang M, Ma X L, Wang J and Zhang F J 2018 *Chin. Phys. B* **27** 058802
- [3] Gao J, Gao W, Ma X, Hu Z, Xu C, Wang X, An Q, Yang C, Zhang X and Zhang F 2020 *Energy Environ. Sci.* **13** 958
- [4] Jouane A, Moubah R, Schmerber G, Lardé R and Odarchenko Y 2018 *Sol. Energy Mater. Sol. Cells* **180** 258
- [5] El-Menyawy E M 2015 *Mater. Sci. Semicond. Proc.* **32** 145
- [6] An Q, Wang J, Gao W, Ma X, Hu Z, Gao J, Xu C, Hao M, Zhang X, Yang C and Zhang F 2020 *Sci. Bull.* **65** 538
- [7] Zhong Y, Zhang Q, Wei Y, Li Q and Zhang Y 2018 *Chin. Phys. B* **27** 078802
- [8] Jouane A, Moubah R, Lassri H, Saifaoui D, Schmerber G, Jaouani H, Ennamiri H, Chapuis Y A and Jouane Y 2016 *Org. Electron.* **39** 138
- [9] Qi B, Zhou Q and Wang J 2015 *Sci. Rep.* **5** 11363
- [10] Mao P, Wei Y, Li H and Wang J 2017 *Nano Energy* **41** 717
- [11] Du Y Y, Lin D Q, Chen G H, Bai X Y, Wang L X, Wu R, Wang J O, Qian H J and Li H N 2018 *Chin. Phys. B* **27** 088801
- [12] Ma X, Wang J, An Q, Gao J, Hu Z, Xu C, Zhang X, Liu Z and Zhang F 2020 *Nano Energy* **70** 104496
- [13] Zhang R C, Wang M Y, Yang L Y, Qin W J and Yin S G 2015 *Chin. Phys. Lett.* **32** 077202
- [14] Ebenhoch B, Thomson Stuart A J, Genevičius K, Juška G and Samuel I D W 2015 *Org. Electron.* **22** 62
- [15] Hu Z, Wang Z, An Q and Zhang F 2020 *Sci. Bull.* **65** 131
- [16] Campbell A J, Bradley D D C and Lidzey D G 1997 *J. Appl. Phys.* **82** 6326
- [17] Ait Ali B, Moubah R, Boulezhar A, Shi S and Lassri H 2020 *Trans. Electr. Electron. Mater.* **21** 436
- [18] Biring S, Sung Y M, Nguyen T P, Li Y Z, Lee C C, Chan A H Y, Pal B, Sen S, Liu S W and Wong K T 2019 *Org. Electron.* **73** 166
- [19] Servaites J D, Ratner M A and Marks T J 2011 *Energ. Environ. Sci.* **4** 4410
- [20] Noh S, Suman C K, Lee D, Kim S and Lee C 2010 *J. Nanosci. Nanotechnol.* **10** 6815
- [21] Yuan H, Song K W, Han C, Tang X Y, He X N, Zhang Y M and Zhang Y M 2019 *Chin. Phys. B* **28** 117303
- [22] Breitenstein O, Altermatt P, Ramspeck K and Schenk A 2006 *Proceedings of the 21st European Photovoltaic Solar Energy Conference, September, 2006*, pp. 625–628
- [23] Qi B and Wang J 2013 *Phys. Chem. Chem. Phys.* **15** 8972
- [24] Chen G, Si C, Tang Z, Guo K, Wang T, Zhang J and Wei B 2016 *Synth. Met.* **222** 293
- [25] Chen G, Wang T, Li C, Yang L, Xu T, Zhu W, Gao Y and Wei B 2016 *Org. Electron.* **36** 50
- [26] Scharber M C, Mühlbacher D, Koppe M, Denk P, Waldauf C, Heeger A J and Brabec C J 2006 *Adv. Mater.* **18** 789
- [27] Oseni S O and Mola G T 2017 *Sol. Energy* **150** 66
- [28] Shockley W and Queisser H J 1961 *J. Appl. Phys.* **32** 510
- [29] Cowan S R, Roy A and Heeger A J 2010 *Phys. Rev. B* **82** 245207
- [30] Alsharari A M, Qashou S I, Darwish A A A and El-Nahass M M 2020 *Thin Solid Films* **704** 137977
- [31] Darwish A A A, El-Shazly E A A, Attia A A and Abd El-Rahman K F 2016 *J. Mater. Sci.: Mater. Electron.* **27** 8786
- [32] Card H C and Rhoderick E H 1971 *J. Phys. D: Appl. Phys.* **4** 1589
- [33] Dogan H and Elagoz S 2014 *Physica E: Low Dimens. Syst. Nanostruct.* **63** 186
- [34] Li J L, Li Y, Wang L, Xu Y, Yan F, Han P and Ji X L 2019 *Chin. Phys. B* **28** 027303
- [35] Li H, He D, Zhou Q, Mao P, Cao J, Ding L and Wang J 2017 *Sci. Rep.* **7** 40134
- [36] Werner J H and Güttler H H 1991 *J. Appl. Phys.* **69** 1522
- [37] Janardhanam V, Jyothi I, Ahn K S and Choi C J 2013 *Thin Solid Films* **546** 63
- [38] Sullivan J P, Tung R T and Pinto M R 1991 *J. Appl. Phys.* **70** 7403
- [39] Altuntaş H, Altundal S, Shtrikman H and Özçelik S 2009 *Microelectron. Reliab.* **49** 904
- [40] Von Wenckstern H, Biehne G, Abdel Rahman R, Hochmuth H, Lorenz M and Grundmann M 2006 *Appl. Phys. Lett.* **88** 92102
- [41] Song Y P, Meirhaeghe Van R L, Laflère W H and Cardon F 1986 *Solid State Electron.* **29** 633
- [42] Chand S and Bala S 2005 *Appl. Surf. Sci.* **252** 358